Effects of ZnO quantum dots on the photostability of acrylate photopolymers used as recording materials

Georgia G Goourey, Pascal Wong-Wah-Chung, Lavinia Balan, Yaël Israëli

Effects of ZnO quantum dots on the photostability of acrylate photopolymers used as recording materials

Georgia G. Goourey[a], Pascal Wong-Wah-Chung[b], Lavinia Balan[c], Yaël Israëli[a*]

[a]*Université Clermont-Auvergne-CNRS-SIGMA, Institut de Chimie de Clermont-Ferrand, Campus des Cézeaux, 24 Avenue Blaise Pascal, TSA 60026, CS 60026, 63178 Aubière Cedex, France*
Email: yael.israeli@uca.fr
[b]*Aix-Marseille Université, Laboratoire Chimie Environnement, CNRS FRE 3416, Europôle de l'Arbois, BP 80, F-13545 Aix-en-Provence Cedex 4*
[c]*Institut de Science des Matériaux de Mulhouse, 15 rue Jean Starcky, BP 2488, F-68057 Mulhouse Cedex*

ABSTRACT

ZnO quantum dots, QDs (5 nm diameter) by their photogenerated charge carriers clearly influence the degradation of the acrylate host matrix, under conditions simulating solar light. As a result, QDs undergo a partial quenching of their fluorescence. To rationalize this influence, the investigation requires understanding the photochemical behavior of the acrylate photopolymer (carrier of ester and ether groups) in the absence of nanofiller. The matrix undergoes simultaneously a post-polymerization and photooxidative degradation. Infrared analysis and headspace gas chromatography coupled with mass spectrometry reveal that the main volatile organic compounds result from the oxidation of the ether groups, supposed to be the primary sites of degradation.

The nanofiller increases the rate of degradation. Also, the concentration of the volatile organic compounds is all the more important as the doping percentage increases. However, the photostability of ZnO/polymer material strongly depends on the size of the nanoparticles. Whereas ZnO QDs display a photocatalytic effect, nanoparticles with a bigger size (10-30 nm) exhibit an unexpected UV-screening effect.

Keywords: acrylate photopolymer; degradation; light exposure; nanocomposite; photostability; ZnO nanoparticles.

1. Introduction

Holographic applications stimulated a constant development of suitable recording media. Photopolymers fulfil most of the requirements that an ideal recording media should satisfy [1,2], and therefore they were considered promising for holographic recording. Recording gratings in photopolymerizable material from imagewise illumination was related to a refractive index modulation Δn (the key for the optical performance) between the constructive and destructive regions of the formed grating. However, in order to develop photosensitive materials with advanced performance (higher Δn), the research was oriented towards phototopolymers doped with dispersed nanoparticles during the last decades. Scientists displayed lots of imagination in investigating this approach; thus TiO_2 [3-6], SiO_2 [6-10], ZrO_2 [6,11-13], ZrO_2:Eu^{3+} [14], $LaPO_4$:Ce^{3+}, Tb^{3+} [15], $LaPO_4$:Tb^{3+} nanorods [16], silver [17,18] and gold nanoparticles [19], CdSe [20], CdSe/ZnS [21,22] and ZnO quantum dots (QDs) [23] were used more or less successfully. During the course of the recording process, nanoparticles were forced to diffuse away from the constructive to the destructive interference regions of the interference pattern [7,11,15-19,21,24].

Since the photopatterned polymer is brought to be exposed to UV light, it is of major importance to consider its photostability as a prerequisite because in general, a polymer is inherently vulnerable to photodegradation (chemical and/or architectural changes) under the conjugated action of oxygen and solar light exposure. Such a degradation results in a deterioration of the performance of the recording material over time. Thus, for commercial applications, it was relevant to assess the photostability of the polymeric matrix. In the present study, the matrix was stemming from the polymerization of a mixture of acrylate monomers consisting of pentaerythritol tetraacrylate (PETTA) and 2-(2-ethoxyethoxy)ethyl acrylate (2EEEA). As a consequence, the whole structure of the synthesized PETTA/2EEEA

copolymer was rather complex and so, assessing its stability required in a first approach to evaluate the resistance to ageing of each of the two homopolymers (carriers of different functional groups) synthesized from the corresponding acrylate monomers [25]. It was established that the combined effect of light and oxygen caused both the post polymerization of the residual vinyl groups of the acrylate units and the degradation of the polymer network. Mainly, from the identification of the volatile organic compounds generated upon UV irradiation, the key elements of the photooxidative degradation of each of the homopolymer were recognized and some pathways of degradation were postulated [25].

The incorporation of ZnO QDs was reported to enhance the optical performance of the grating [23] but one could wonder about the specific sensitizing effect of ZnO nanoparticles on the polymeric matrix upon UV irradiation. This question is of paramount importance since the influence of these nanoparticles on the photostability of nanocomposite materials was not clear. As can be seen through the following examples, previous studies carried out on a variety of polymers containing ZnO nanoparticles revealed both a photoprotective and photocatalytic effect depending on the host matrix.

In the case of poly(vinyl chloride) (PVC), ZnO could photocatalyse the degradation in aqueous medium under oxygen of air and light [26,27]. In the presence of oxygen or water, the photogenerated hole-electron pairs could yield hydroxyl radicals $HO^{\bullet}$. These active radicals, free or at the surface of ZnO, might initiate the partial degradation of PVC by hydrogen abstraction from the polymer backbone. The resulting PVC radicals would further yield some photoproducts by subsequent reactions.

In the case of polyurethane, light and oxygen induced the loss of the urethane groups through oxidative reactions, thus entailing mass loss and chain scission reactions [28]. Incorporating ZnO nanoparticles (20, 40 or 60 nm diameter) was reported to boost the degradation with a rate all the more important as their concentration was higher and their size

smaller [29]. This feature was explained as an interface related phenomenon. This latter especially enhances as the nanoparticle interfacial areas increased [29]. Whatever the experimental conditions (irradiation at different relative moisture degrees [29-31] or with cycles of water spray and drying [32]), the degradation was always ascribed to the photocatalytic effect of ZnO [29-32].

This prodegradant effect also occurred for glass fiber reinforced unsaturated polyester; ZnO catalyzed the decarbonylation process by cleavage of C-O bond on the surface [33]. A recent study performed in polylactide/ZnO nanocomposites [34] has demonstrated that with increasing doping percentage 1) the rate of oxidation enhanced and 2) the oxidation became more and more superficial. This latter feature was a consequence of the limitation of the penetration of light into the sample which was ascribed to the UV-screen effect of ZnO.

For polypropylene nanocomposites, ZnO (50 nm diameter) acted as a stabilizer [35,36]; the higher was the content of nanoparticles, the lower was the carbonyl index used as a probe of the degradation of the polymeric matrix. As a consequence, the surface of the irradiated material exhibited little cracks and the mechanical properties were improved compared to the undoped irradiated material [35,36]. Concerning low density polyethylene, in some studies ZnO was reported to delay the photodegradation (commercial ZnO, 20 nm diameter and loading 2%) [37] or to promote the degradation (synthesized ZnO, 30 nm diameter, loading less than 1 %) [38].

So, based on the literature, it appeared that the durability of a new polymer material requires assessing the effect of ZnO nanoparticles on its long term lifetime. In this context, the first part of the present work aimed at evaluating the photostability of PETTA/2EEEA polymer in conditions simulating solar light. The second and third parts of this work were devoted to investigating the influence of nanofillers on the photostability of acrylate photopolymer (PETTA/2EEEA copolymer). Analysis using infrared and fluorescence

spectroscopy, and headspace gas chromatography coupled with mass spectroscopy were carried out in order to follow up and characterize the chemical changes of the polymeric matrix and to determine the involvement of ZnO nanoparticles in the degradation process.

2. Experimental section

2.1. Materials

Pentaerythritol tetraacrylate (PETTA) and 2-(2-ethoxyethoxy)ethyl acrylate (2EEEA) monomers (Fig. 1) were purchased from Aldrich and used as received without further purification.

Fig. 1

Two types of oleic acid-functionalized ZnO nanoparticles were used. The first ones (10-30 nm diameter, 99 % purum) were delivered from SkySpring Nanomaterials and were used without further purification. The second ones, ZnO quantum dots (QDs) (3-5 nm diameter) were synthesized through a sol-gel route [39-41]. Anhydrous zinc acetate $Zn(OAc)_2$ (1.2 mmol) (Sigma-Aldrich, purum 99.99 %) was introduced in 20 mL of absolute ethanol under nitrogen atmosphere. The mixture was heated at 50 °C until complete dissolution of $Zn(OAc)_2$. Then, oleic acid (0.22 mmol) (Sigma-Aldrich, purum > 98 %) was added and the mixture was heated to reflux. In parallel, in a separate flask, tetramethylammonium hydroxide (TMAH) (1.99 mmol) (from Sigma-Aldrich, a methanolic solution (25 wt %)) was dissolved in 5 mL of refluxing absolute ethanol. This solution was quickly injected in the mixture of $Zn(OAc)_2$ and oleic acid, then refluxed for 2 minutes, diluted with 50 mL of ethanol and finally cooled at 0°C. A white precipitate was observed and, after 15 minutes at 0 °C, the colloidal suspension was centrifuged and the supernatant was discarded. The precipitate of

oleate capped ZnO QDs was washed several times with ethanol; it was kept as a suspension in ethanol and stored in the dark at 4 °C.

The typical photopolymerizable formulations were prepared in low-light conditions by mixing the two acrylate monomers (80:20 PETTA:2EEEA) with a photoinitiator (dl-camphorquinone [CQ] from EGA Chemie, 1.5 wt%) and a co-initiator (ethyl 4-dimethylaminobenzoate [DABE] from Aldrich, purum > 99 %, 0.6 wt%). 1 or 5 wt% of ZnO was then added and the dispersion was homogenized by magnetic stirring for two days. In parallel, ethanol was removed by bubbling nitrogen through the formulation.

The polymer samples were prepared by coating the photopolymerizable mixture onto a glass slide or a CaF_2 plate or, on a small aluminum rectangular crucible, followed by irradiation performed in an inert argon gas atmosphere using a conventional irradiation device (monochromator) at 488 nm with an intensity of 0.6 mW cm^{-2}, in the same conditions used for recording [23].

2.2. Experimental set-up and procedure

For photoageing investigations, two ageing simulator devices were used. The first one was a SEPAP 14/24 unit equipped with a medium pressure mercury lamp (Novalamp RVC 400W). The source was located along one of the focal axis of a cylinder with an elliptical base. The samples were arranged on a rotating carousel that could receive 15 samples, located at the other focal axis. Experiments were performed at 40 °C. The second ageing device was a SEPAP 12/24 unit from Atlas, equipped with four medium pressure mercury lamps (Novalamp RVC 400 W) located in a vertical position at each corner of the chamber. Wavelengths below 295 nm were filtered by the glass envelope of the sources. A rotating

carousel, on which the samples were fixed, was placed at the center of the chamber. The temperature at the surface of the sample was fixed at 60 °C.

Infrared spectra were recorded on a Nicolet 5SXC FTIR spectrometer with Omnic software. Spectra were obtained with a 4 cm^{-1} resolution and 32 scan summation. IR-ATR (Attenuated Total Reflectance) spectra were recorded with a Nicolet 380-ATR spectrophotometer equipped with a Thunderdome-ATR (4 cm^{-1}, 32 scans). The Thunderdome is a single reflection ATR accessory with a Diamond crystal (depth penetration ≈ 3-5 µm). To ensure fair reproducibility, each measurement was repeated on different areas of the polymer. UV-visible absorption and fluorescence spectra (excitation wavelength = 350 nm) were recorded on a Shimadzu UV-2101 PC and a Perkin Elmer LS55 spectrophotometer, respectively.

The photo-IR combines light irradiation and infrared analysis using a Hamamatsu light generator equipped with a medium pressure Xe/Hg source (Lightningcure LC6 1W) and Thermo Optek Nexus FTIR spectrometer. The source was filtered by a sapphire disk to deliver wavelengths representative of outdoor ageing ($\lambda \geq 300$ nm). The films (deposited on an aluminium rectangle crucible) were first placed in a sealed gas cell that was located in the infrared analysis cavity equipped with an oven, and then were irradiated *in-situ* [42]. The temperature in the oven was maintained constant at 40 °C. The infrared spectra of the released gas were collected every two hours during 60 hours with a 4 cm^{-1} resolution and 32 scan summation.

For solid-phase microextraction (SPME) experiments, the photopolymer films (deposited on an aluminum rectangle crucible) were irradiated in the SEPAP 12/24 unit, in 20 mL sealed vials to collect the volatile organic compounds (VOCs) stemming from the photodegradation. Carboxen–PDMS fiber (75 µm) purchased from Supelco (Bellefonte, PA, USA) was used to extract the volatile organic compounds (VOCs) in the headspace (HS) [43-44]. VOCs were

analyzed using SPME coupled with gas chromatography/mass spectrometry (GC-MS) as previously described in details in reference [43]. Mass spectra and reconstructed chromatograms (total ion current, TIC) were acquired under the electron ionization mode (EI) at 70 eV and recorded from 20 to 400 *m/z*. The compounds were identified by comparison with the mass spectra of the spectral library.

VOCs stemming from the *in-situ* irradiation of the photopolymer sample were also analyzed by using a purge and trap dynamic headspace extraction coupled with polychromatic irradiation and GC-MS system. This apparatus is well described in a previous work [25].

A nanoscope IIIa atomic force microscope (AFM) from Veeco Instruments was used for nanoindentation. Changes of the mechanical properties were followed versus irradiation time using AFM nanoindentation. The force-distance curves were monitored under a constant deflection or constant loading. Nanoindendations were carried out using a Berkovitch-like diamond tip (resonance frequency of 64.05 kHz and a curvature radius of 25 nm) mounted onto a stainless steel cantilever with a spring constant of 204.5 $N.m^{-1}$. To ensure a good reproducibility five nanoindentation tests in different areas of the polymer were performed. Each test corresponded to five indentations, thus 5 x 5 force curves were used with forces between 4 and 20 µN.

The nano-hardness was determined by using a procedure developed by Oliver and Pharr [45,46]. This latter was based on the Sneddon's approach, in which the force, F was given as a power law of the displacement, h: $F(h) = \alpha h^m$ where α and m were constants depending on the mechanical properties of the sample and the tip geometry [47].

The force-displacement curve, F(z) must first be converted into a force-indentation curve, F(h) where z and h are the piezo displacement and the indentation depth, respectively. z is converted into h according to the following relationship [46]: $h = z - d = z - \frac{F}{k}$ where k designates the spring constant of the cantilever.

Then, the contact depth, h_c can be calculated using the relationship: $h_c = h_{max} - \frac{\varepsilon F_{max}}{S}$ where S is the slope of the unloading curve and ε is a parameter which depends on the indenter geometry (for a Berkovitch tip, ε = 0.75). The contact depth is then used to determine the area function A(h_c): $A(h_c) = 24.56h_c^2$. From the initial slope of the unloading curve, as the indenter head was withdrawn from the surface, the reduced elastic modulus can be determined from the relationship: $E_r = \frac{S}{2\beta}\sqrt{\frac{\pi}{A(h_c)}}$ where β is a parameter depending on the indenter geometry (for a Berkovitch tip, β = 1.034). The Young's modulus E can be calculated from the reduced modulus.

Finally, the nano-hardness H is defined by the following relationship: $H = \frac{F_{max}(h_{max})}{A(h_c)}$.

3. Results and discussion

3.1. Photostability of the photopolymer

3.1.1 Chemical modifications

The chemical modifications of the obtained PETTA/2EEEA photopolymer (deposit on a CaF_2 plate) were monitored by transmission infrared spectroscopy during 100 hours of exposure under accelerated photoageing conditions. The main changes were reported in Table 1. Light exposure caused the post-polymerization of the residual vinyl groups of the acrylate units. This fact was underlined by the decrease of the absorption bands at 3037, 1635 and 1408 cm^{-1} and the concomitant development of new bands at 2935 and 1452 cm^{-1} assigned to methylene groups. Such post-polymerization was also observed in previous studies performed on the two homopolymers synthesized from the photopolymerization of the corresponding

acrylate monomers [25]. It is relevant to mention that the same experiment performed in the absence of oxygen also led to the same features. Moreover, the kinetic evolution of the consumption of the residual vinyl groups of the acrylate units was identical whether the experiment was carried out in air or in inert atmosphere. Both the consumption of ether and ester functions and the formation of new functional groups (hydroxyl at 3320 cm^{-1} and carbonyl at 1782 cm^{-1}) on the polymeric backbone pointed out that light and oxygen exposure entailed a photo-oxidation of the material. This photooxidative degradation occurred simultaneously with the post-polymerization reaction.

Table 1

Elucidating the degradation mechanism required gaining a better insight into the chemical modifications of the material. For this purpose, most of the oxidation products could be identified by chemical derivatization treatments [48]. Unfortunately, in the present study such a treatment did not induce any change in the infrared spectra. However, the loss of the ether groups suggested that these groups are involved in the degradation process. This fact was supported by previous studies carried out in homo-2EEEA, which revealed that the homopolymer degraded mainly through chain scission and hydrogen abstraction reactions. These reactions accounted for the generation of volatile organic compounds [25]. They were also expected to occur in PETTA/2EEEA polymer. Thus, in the next part of this work, our attention focussed on the gases stemming from the irradiation of the polymer.

Photo-IR analysis showed the release of carbon monoxide and carbon dioxide (Fig. 2a). These gases were also detected in the case of the irradiation of homo-PETTA and homo-2EEEA [25]. Their formation was explained by chain scission reactions (Norrish I cleavage and ester elimination reactions) that took place both on PETTA and 2EEEA units [49,50]. In the 1300-600 cm^{-1} domain, new absorption bands developed and they were assigned amongst others, to C-O-C bond vibrations (Fig. 2b).

Fig. 2

The comparison between the photo-IR spectra of the gases arising from *in-situ* irradiation of PETTA/2EEEA and homo-2EEEA films revealed a similarity in the 1300-600 cm^{-1} region [25]. This feature seemed to suggest that 2EEEA units might be the prime sites of the degradation process and therefore, the responsible for the instability of the copolymer.

In order to confirm this hypothesis and to gain better understanding in the photochemical modifications of the polymer matrix, an approach based on the identification of the volatile organic compounds by HS-SPME/GC-MS was used. Fig. 3a displays the evolution of the chromatogram of a headspace of a film at irradiation times ranging from 10 to 150 hours. Various low molecular weight compounds migrated in the gas phase and were mainly identified with high confidence index (Table 2). It must be emphasized that the volatile compounds, formed after 10 hour-exposure and beyond, were identical to those stemming from the photo-oxidation of homo-2EEEA [25]. This corroborates the fact that 2EEEA units were responsible for the instability on PETTA/2EEEA film. This source of instability had already been recognized in several systems containing ether groups [49,51-53].

Fig. 3

Table 2

Fig. 3b displays the kinetic evolution of the area of the peaks corresponding to ethanoic acid and 2-(2-ethoxyethoxy)ethanol. Whereas the acid accumulated in the medium, the concentration of 2-(2-ethoxyethoxy)ethanol increased, passed through a maximum and after 10 hours of irradiation, decreased and tended to zero for longer irradiation times. Such a behavior suggested that this species in turn would undergo photo-oxidation initiated by hydrogen abstraction in the α position with respect to oxygen atom, in accordance with the proposed mechanism of Fig. 4. The two degradation pathways (1 and 2) led to radicals that would react with oxygen. The resulting species would then, abstract labile hydrogen to

2EEEA units gaving rise to unstable hydroperoxides. The obtained alkoxy radicals would undergo a β−scission reaction. C_2H_5-O-CH_2CH_2-$O^{\bullet}$ radicals, formed from route 1 would abstract a hydrogen from PH, thus leading 2-ethoxyethanol. The β−scission reaction occurring through route 2 generated the formation of ethanal that could in turn oxidize in ethanoic acid [54]. 2-ethoxyethanol could subsequently undergo photo-oxidation through a mechanism similar to that proposed for 2-(2-ethoxyethoxy)ethanol yielding ethanoic acid. So, this acid would not only result from the oxidative degradation of 2EEEA units but also from the photochemical instability of 2-(2-ethoxyethoxy)ethanol and 2-ethoxyethanol. This feature might explain the increasing release of ethanoic acid (Fig. 3b) and the irregular kinetic evolution of 2-ethoxyethanol (compound E) as shown in Fig. 3a.

Fig. 4

3.1.2. Surface mechanical properties

In general, the chemical modifications of a polymer under light and oxygen exposure were the results of chain scissions and crosslinking reactions (recombination of macroradicals). It was established in the previous section that chain scission accounted for the stemming of volatile organic compounds. However, at this stage, one could wonder whether PETTA/2EEEA polymer also underwent crosslinking. The chemical modifications could induce changes in the mechanical properties of polymer films. These latter are generally monitored by dynamic mechanical analysis (DMA) [55, 58]. However, it was mentioned in the literature that AFM-nanoindentation was an alternative technique to DMA [59, 60]. From investigations performed on ten polymers, chosen for their wide range of elastic modulus, Lee has demonstrated that AFM nanoindentation was a relevant tool to measure mechanical properties in terms of hardness and Young's modulus [59]. In the same way, the modifications of the harness and the Young's modulus of a thermoset coating, as the result of

the photodegradation, were followed by this technique [60, 61]. Taking into account of the literature, we have chosen to perform nano-hardness measurements from AFM nanoindentation. As an example, the force-distance curves are represented in Fig. 5a before irradiation and after 50 and 300 hours of irradiation. The figure points out that exposure to light and oxygen caused the shift of the loading/unloading curves to the left with a noticeable decrease of the hysteresis, which indicated an increase of the nano-hardness. Indeed, the kinetic evolution of calculated hardness values given for a constant load of 20 µN in Fig. 5b, showed that the nano-hardness increased by a factor of ca 8.5. It strongly varied from 40 ± 10 MPa before irradiation to 330 ± 10 MPa after 50 hours of irradiation. This important increase was mainly ascribed to the post-polymerization of the residual vinyl groups of the acrylate units as highlighted by transmission infrared analysis reported above. This feature was confirmed by the linear correlation between the evolution of the nano-hardness and the decay of the absorbance of the band at 1635 cm^{-1} corresponding to vinyl groups (Inset of Fig. 5b). Beyond 50 hours, the additional densification of the network showed a weak evolution from 330 ± 10 MPa to 350 ± 20 MPa after 50 and 300 hours of irradiation, respectively. Such a result could reflect a recombination of macroradicals that led to crosslinking.

Fig. 5

In terms of Young's modulus, visually the slope (S) of the unloaded curve which could be directly related to the reduced elastic modulus, underwent noticeable changes from 0 to 50 hours of irradiation indicating that in this period the sample was more rigid. Even if AFM-nanoindentation, in this study, allowed to obtain partial data regarding to mechanical properties, these latter contributed to gain better understanding in the photochemical modifications of the polymer matrix.

3.2. Influence of ZnO QDs on the phostability of the photopolymer

3.2.1. Chemical modifications

To determine the contribution of ZnO quantum dots in the degradation process, the chemical modifications of the pure photopolymer (without QDs) and the composite material (1 wt% of QDs), deposited on a glass plate, were monitored by ATR-IR. It is worthy of notice that the changes detected by ATR-IR were similar to those observed in the case of the bulk analysis (deposit on a CaF_2 plate, film thickness of 12 ± 1 µm) performed by transmission infrared spectroscopy. This similar behaviour confirms that the photo-oxidation of the material occurred not only at the surface of the samples but also in the bulk.

Fig. 6a shows the evolution of the ATR-IR spectra in the 1900-900 cm^{-1} in the course of irradiation in accelerated conditions. A drastic decrease of the bands was observed. To account for the influence of nanoparticles, the kinetic evolution of the decay of ester groups (C=O band at 1724 cm^{-1}) in the pure matrix was compared with that of a photopolymer containing dispersed QDs (Fig. 6b). This comparison pointed out a clear influence of quantum dots on the kinetics of degradation attributed to the photocatalytic effect. Indeed, while some 20 % of the ester groups were consumed after 15 hours of irradiation in the composite material, the same percentage was attained after 100 hours of irradiation in the absence of QDs.

Fig. 6

Since the band at 1153 cm^{-1} corresponds to the stretching vibrations of the C-O bonds of the ester groups, a linear correlation between the two bands of the ester groups at 1724 and 1153 cm^{-1} should be expected. The inset of Fig. 6b shows that a linear correlation was observed whether ZnO QDs were present (1 wt%) or not.

In a following step, the influence of the doping percentage of semi-conductor nanocrystals on the composition of the gases stemming from the degradation of the polymer matrix was

examined. For this purpose, three sample containing increasing amounts of QDs (0, 1 and 5 wt %) were analyzed by HS-SPME/GC-MS. For 10 and 150 hours of irradiation in an accelerated artificial ageing device (SEPAP 12/24), the TIC chromatograms, obtained for the three materials, were compared (Fig. 7a). It turns out that the higher the doping percentage in the matrix was, the lower concentration in the evolved gas phase was. By way of illustration, Figure 7b shows this behaviour in the case of 2-(2-ethoxyethoxy)ethanol (compound J). Similarly, the formation of ethanoic acid (compound H) drastically decreased in the presence of ZnO QDs (Fig. 7a)

Fig. 7

In order to better encircle the role played by the nanoparticles in the photo-oxidation mechanism, a purge and trap dynamic headspace extraction coupled with a polychromatic *in-situ* irradiation and GC-MS systems was used to follow the kinetics of formation of the gases at shorter exposure times. The detected species were ethanal (1.8 min), ethanol (compound B, 4.0 min), 2-ethoxyethanol (E, 16.5 min) and 2-(2-ethoxyethoxy)ethanol (J, 23.8 min). Ethanal clearly evidenced by this technique would subsequently oxidize to ethanoic acid. From these *in-situ* GC-MS experiments, it was observed that increasing amounts of ZnO QDs mainly favoured the accumulation of ethanol and 2-(2-ethoxyethoxy)ethanol in the gaseous phase (Fig. 8). These results confirmed that the semi-conductor nanocrystals mainly affected the photochemical behaviour of the polymer through their photocatalytic effect.

Fig. 8

Hydroxyl radicals are known to be the main reactants in the photocatalytic process. This species resulted from reaction occuring between the photogenerated hole-electron pairs and, water and O_2 molecules [62-64]. Despite the fact that the studied acrylate photopolymer was hydrophobic, the presence of hydrophilic groups such as C=O and CH_2CH_2O allowed sorption of water molecules [65-67]. Thus, the higher amount of particles in the polymer is,

the higher concentration of $HO^{\bullet}$ is and finally the more important the photocatalytic effect is. This feature is illustrated in Fig. 8b by the increasing concentration of 2-(2-ethoxyethoxy)ethanol with increasing the amount of QDs. Knowing that Norrish I and ester elimination reactions (scission reactions) could account for the formation of this compound, to explain such a behavior (Fig. 8b), one could hypothesize a hydrogen atom abstraction at β position of the C=O by $HO^{\bullet}$, as illustrated in Fig. 9. The resulting macroradicals would evolve into macroalkoxy radicals through the formation and the decomposition of hydroperoxides. β-scission reaction would give rise to radicals that in turn undergo a decarboxylation process. Under oxygen and light exposure, the obtained radicals would subsequently yield 2-(2-ethoxyethoxy)ethanol.

Fig. 9

Denisyuk *et al* [68] studied the photopolymerization of acrylate monomers at 365 nm in the presence of ZnO nanoparticles (20 nm diameter). They proposed a mechanism accounting for the role played by ZnO in the photoinitiation step (see Fig. 5 in reference 68). This mechanism involved photogenerated holes that abstracted hydrogen from vinyl groups of the monomers (H at β position of the C=O). Contrary to what was reported by Denisyuk [68], the presence of QDs did not affect the kinetics of the post-polymerization of PETTA/2-EEEA (not shown).

3.2.2. Surface mechanical properties

According to the literature [32], in the vicinity of nanoparticles, the polymer degraded faster. Some cracks were initiated at the polymer/particle interface and then propagated in the depth of the sample thus leading to removal of the matter. Under the prevailing experimental conditions, the ZnO doped photopolymer exhibited cracks after 60 hours of irradiation compared to 100 hours in the case of undoped polymer.

In order to rationalize the influence of the nanoparticles on the mechanical properties of the composite materials (1 wt% of ZnO QDs), the nano-hardness was measured using AFM upon irradiation. The values were compared with the ones obtained in the case of the undoped polymer for irradiation times ranging from 0 to 50 hours; beyond 50 hours, the doped polymer became cracked. The weak difference observed before irradiation (Table 3) for the samples was not significant since it was within the accuracy range. The results reported in Table 3 revealed that the presence of ZnO quantum dots did not affect the kinetic evolution of the nano-hardness. This observation is in perfect agreement with what was previously established: 1) the increase of the nano-harness of undoped polymer is mainly related to the post-polymerization of residual acrylate vinyl groups (Fig. 5b), and 2) the presence of nanoparticles did not modify the kinetics of post-polymerization (not shown).

Table 3

3.2.3. Fluorescence properties

ZnO quantum dots exhibit a green-yellow fluorescence emission attributed to defects located at the surface [69,70]. The recombination of the photogenerated electrons in the shallow trap level with the holes in deep trap level could be responsible for this emission [69,71-73]. Nevertheless, it is worth mentioning that the origin of this fluorescence was subject to controversy. Anyway, whatever the mechanism of defect emission, if the photogenerated charge carriers were involved in the degradation process, one should expect a partial or complete quenching of this fluorescence. After 30 minutes of irradiation, a total extinction of the fluorescence at 570 nm ($\lambda_{exc.}$ = 350 nm) was observed and in parallel, a new emission developed at 390 nm. However, the fluorescence emission was recovered after 3 days of storage in the dark and at room temperature. This point will be discussed later. It was verified that the excitation spectrum under emission at 570 nm effectively corresponded to

ZnO QDs absorption (Fig. 10a). The species responsible for the emission at 390 nm was not identified yet.

Fig. 10b displays the evolution of the fluorescence emission after irradiation and storage in the dark during one, two and three days. It shows the partial quenching of the visible fluorescence of the nanoparticles. Interestingly, the residual fluorescence linearly correlated with the decrease of the ester functions of the photopolymer (band at 1724 cm^{-1}) (Inset of Fig. 10b), as expected. This correlation corroborated the involvement of electron-hole pairs in the mechanism of photo-oxidation of the polymeric matrix.

Fig. 10

According to the literature [74,75], the extinction, observed after irradiation, was attributed to a photoinduced electron accumulation process due to the lack of oxygen in the bulk of the material. This excess of electrons prevented the recombination with green emission. The partial recovery of the emission when the irradiated sample was stored in the dark might be accounted for the slow diffusion of oxygen in the depth of the samples. Oxygen might act as an electron scavenger and prevent the charges from accumulating in the conduction band [74].

3.3. Influence of the size of ZnO nanoparticles on the phostability of the photopolymer

As part of their investigations on ZnO-polyurethane, Gu *et al* [76] evidenced the role played by the polymer/nanoparticle interface in the photodegradative process of the polymer matrix. They showed that the higher the amount of ZnO in the media, or the lower the nanoparticle size was, the more pronounced the photocatalytic effect and the degradation were. To rationalize these observations, they assumed that the properties of the polymer were different at the interface and in the bulk [76]. With an approach aiming at evaluating the

influence of the size of ZnO QDs on the oxidative degradation of the polymer, two types of particles were used: synthesized QDs, 5 nm diameter and commercial NPs, 10-30 nm diameter.

ATR-IR analysis revealed that the chemical modifications of the matrix strongly depended on the size of nanoparticles. The initial rate of degradation of the polymer was determined in the absence of ZnO and in the presence of 1 wt% of nanoparticles using the ester groups (band at 1724 cm^{-1}) as a probe. The results are reported in Table 4.

Table 4

First, it must be observed that the rate of degradation decreased by a factor of ten by addition of ZnO NPs compared to the reference undoped system while it increased by roughly a factor of 2 with ZnO QDs. To confirm these results, the samples were also analyzed by infrared spectroscopy in transmission mode and the same influence of the size of the nanoparticles on the degradation rate was observed. So, the nanoparticles with the biggest size seemed to act as protectors against photoinduced degradation of the polymeric matrix. This unexpected behavior is not consistent with what was reported by Gu *et al* on ZnO-polyurethane systems [76].

If ZnO-NPs exhibit a protective action against the photodegradation, this effect should go along with a modification of the HS-SPME/GC-MS chromatograms. Indeed, after 150 hours of exposure, the chromatograms of volatile organic compounds stemming from the irradiation of the undoped polymer and of the composite material (1 wt% ZnO NPs, size 10-30 nm) were similar (Fig. 11a) while only ethanoic acid (compound H) was generated in the sample doped with ZnO QDs (Fig. 11). To get a better idea of the influence of nanoparticles, we focused on 2-ethoxyethanol (compound E) and ethanoic acid. The evolution of the area of the peak of compound E as the function of the size of the nanoparticles is given in Fig. 11b. The following tendency was observed: the area obtained for the composite with 1 wt% NPs 10-30

nm diameter was higher than the area for pure polymer which was itself, higher than that of material with 1 wt% QDs, 5 nm diameter. This tendency corroborated the conclusions issued from infrared spectroscopy analysis, i.e.nanoparticles of 10-30 nm diameter played a photoprotector role in our experimental conditions.

Fig. 11

Ethanoic acid not only resulted from the photo-oxidation of the 2EEEA but also from the subsequent oxidation of degradation products. Whereas in the case of pure photopolymer, this species accumulated in the gas phase, in the presence of ZnO QDs, it underwent a photocatalytic degradation responsible of its low production as shown in Fig. 11. According to the literature, the photocatalytic degradation of ethanoic acid proceeded both in liquid and gas phase [77, 78]. The degradation occured by decarboxylation and by oxidation involving the holes and the hydroxyl radicals. Besides, ab initio calculations underlined that the main degradation pathway with the hydroxyl radicals was the abstraction of the acidic hydrogen, at the carboxylic acid side. The hydrogen abstraction resulted in the corresponding radical which may decompose into CO_2 and the CH_3 radical [79].

4. Conclusions

The durability of a new ZnO/acrylate polymer material requires investigating the effect of the nanofillers on its long term lifetime. This assessment passes first through the understanding of the photochemical behavior of undoped PETTA/2EEEA polymer upon exposure under conditions simulating solar light. During the course of the irradiation, the copolymer simultaneously underwent a post-polymerization and a photo-oxidation. These phenomena led to chemical modifications (loss of the residual vinyl groups, of the ester and

ether functions and, the formation of photoproducts in the macromolecular backbone and of volatile organic compounds) and to surface mechanical properties changes (particularly nano-hardness). In particular, 2EEEA units contributed to the instability of the copolymer towards the photodegradation.

Then, a particular attention was paid to the influence of ZnO quantum dots, QDs (5 nm diameter) on the degradation of the host matrix. On the one hand, the study revealed that QDs did not modify the kinetics of the post-polymerization. On the other hand, it pointed out that the nanoparticles acted as a photocatalyst involving the generated hole-electron in the degradation process. As a consequence, QDs underwent a partial quenching of their green yellow fluorescence. Introducing 1 wt% of quantum dots boosted 1) the rate of degradation; this latter doubled by comparison with the one in the case of the undoped PETTA/2EEEA copolymer, 2) the development of the cracks and, 3) the formation of volatile organic products. The quantity of the released gas was all the more important as the doping percentage increased.

Finally, the photostability of the polymeric matrix strongly depended on the size of the nanofillers. Indeed, ZnO nanoparticles of 10-30 nm diameter exhibited an unexpected photoprotective effect on the degradation contrary to their counterpart quantum dots (5 nm diameter). Introducing 1 wt% led to a decrease of the rate of degradation by a factor of 10 by comparison with that of the undoped polymer. Concerning the post-polymerization process, whatever the size of the nanoparticles, its kinetics remained unchanged.

As previously mentioned in the literature, this investigation is all the more important as the role played by ZnO nanoparticles towards the photostability could not be predicted. Besides, this assessment is relevant for the design and reliability of composite materials with required properties in their service life.

Acknowledgements

Drs Sébastien Berthumeyrie and Pierre-Olivier Bussière are gratefully thanked for their help in AFM nano-indentation measurements. Florence Delor-Jestin is thanked for photo-IR analysis.

References

[1] L. Dhar, K. Curtis, A. Hale, M. Schnoes, W. Wilson, M. Tackitt, A. Hill, M. Schilling, H. Katz, in: M. Hill (Ed.), High density holographic data storage, Bell Laboratories & Lucent Technologies, New Jersey, 2000, pp. 457-465.

[2] D. Jurbergs, F.-K. Bruder, F. Deuber, T. Fäcke, R. Hagen, D. Hönel, T. Rölle, M.-S. Weiser, A. Volkov,New recording materials for the holographic industry, in H.I. Bjelkhagen, R.K. Kostuk (Eds.), Practical Holography XXIII: Materials and Applications, Proc. of SPIE 2009, Vol. 7233, pp. 72330K-1-72330K-10.

[3] C. Sánchez, M.J. Escuti, C. van Heesch, C.W.M. Bastiaansen, D.J. Broer, J. Loos, R. Nussbaumer, TiO_2 Nanoparticle-photopolymer composites for volume holographic recording, Adv. Funct. Mater. 15 (2005) 1623-1629.

[4] O.V. Sakhno, L.M. Goldenberg, J. Stumpe, T.N. Smirnova, Surface modified ZrO_2 and TiO_2 nanoparticles embedded in organic photopolymers for highly effective and UV-stable volume holograms, Nanotechnology 18 (2007) 105704-1-105704-7.

[5] T.N. Smirnova, L.M. Kokhtich, O.V. Sakhno, J. Stumpe, Holographic nanocomposites for recording polymer–nanoparticle periodic structures: I. General approach to choice of components of nanocomposites and their holographic properties, Opt. Spectrosc. 110 (2011) 129–136.

[6] N. Suzuki, Nanoparticle-dispersed photopolymer for volume holographic recording, Ph.D. Thesis, The University of Electro-Communications, Tokyo, Japan, 2007.

[7] Y. Tomita, K. Chikama, Y. Nohara, N. Suzuki, K. Furushima, Y. Endoh, Two-dimensional imaging of atomic distribution morphology created by holographically induced mass transfer of monomer molecules and nanoparticles in a silica-nanoparticle-dispersed photopolymer film, Opt. Lett. 31 (2006) 1402-1404.

[8] T. Juhl, J.D. Busbee, J.J. Koval, L.V. Natarajan, V.P. Tondiglia, R.A. Vaia, T.J. Bunning, P.V. Braun, Holographically directed assembly of polymer nanocomposites, ACS Nano 4 (2010) 5953-5961.

[9] S. Han, M. Lee, B.K. Kim, Effective holographic recordings in the photopolymer nanocomposites with functionalized silica nanoparticle and polyurethane matrix, Opt. Mater. 34 (2011) 131-137.

[10] E. Hata, K. Mitsube, K. Momose, Y. Tomita, Holographic nanoparticle-polymer composites based on step-growth thiol-ene photopolymerisation, Opt. Mater. Express 1 (2011) 207-222.

[11] G. Garnweitner, L.M. Goldenberg, O.V. Sakhno, M. Antonietti, M. Niederberger, J. Stumpe, Large-Scale Synthesis of organophilic zirconia nanoparticles and their application in organic–inorganic nanocomposites for efficient volume holography, Small 3 (2007) 1626–1632.

[12] K. Chikama, K. Mastubara, S. Oyama, Y. Tomita, Three-dimensional confocal Raman imaging of volume holograms formed in ZrO_2 nanoparticle-photopolymer composite materials, J. Appl. Phys. 103 (2008) 113108-1–113108-6.

[13] K. Omura, Y. Tomita, Photopolymerization kinetics and volume holographic recording in ZrO_2 nanoparticle-polymer composites at 404 nm, J. Appl. Phys. 107 (2010) 023107-1–023107-6.

[14] T. Ninjbadgar, G. Garweitner, A. Börger, L.M. Goldenberg, O.V. Sakhno, J. Stumpe, Synthesis of luminescent ZrO_2:Eu^{3+} nanoparticles and their holographic sub-micrometer patterning in polymer composites, Adv. Funct. Mater. 19 (2009) 1819–1825.

[15] O.V. Sakhno, T.N. Smirnova, L.M. Goldenberg, J. Stumpe, Holographic patterning of luminescent photopolymer nanocomposites, Mater. Sci. Eng. C 28 (2008) 28–35.

[16] A. Barichard, L. Frezet, A. Potdevin, G. Chadeyron, Y. Israëli, Influence of hydrothermally-synthesized $LaPO_4:Tb^{3+}$ nanorods on the physical and physico-chemical properties of photo-structured acrylate material, Mater. Chem. Phys. 141 (2013) 138–144.

[17] T.N. Smirnova, L.M. Kokhtych, A.S. Kutsenko, O.V. Sakhno, J. Stumpe, The fabrication of periodic polymer/silver nanoparticle structures: *in situ* reduction of silver nanoparticles from precursor spatially distributed in polymer using holographic exposure, Nanotechnology 20 (2009) 405301-1-405301-11.

[18] L. Balan, C. Turck, O. Soppera, L. Vidal, D.J. Lougnot, Holographic recording with polymer nanocomposites containing silver nanoparticles photogenerated in situ by the interference pattern, Chem. Mat. 21 (2009) 5711–5718.

[19] L.M. Goldenberg, O.V. Sakhno, T.N. Smirnova, P. Helliwell, V. Chechik, J. Stumpe, Holographic composites with gold nanoparticles: nanoparticles promote polymer segregation, Chem. Mater. 20 (2008) 4619–4627.

[20] X. Liu, Y. Tomita, J. Oshima, K. Chikama, K. Matsubara, T. Nakashima, T. Kawai, Holographic assembly of semiconductor CdSe quantum dots in polymer for volume Bragg grating structures with diffraction efficiency near 100%, Appl. Phys. Lett. 95 (2009) 261109-1–261109-3.

[21] A. Barichard, T. Galstian, Y. Israëli, Influence of CdSe/ZnS quantum dots in the polymerization process and in the grating recording in acrylate materials, J. Phys. Chem. B. 114 (2010) 14807–14814.

[22] A. Barichard, T. Galstian, Y. Israëli, Physico-chemical role of CdSe/ZnS quantum dots in the photo-polymerization process of acrylate composite materials, Phys. Chem. Chem. Phys. 14 (2012) 8208–8216.

[23] G.G. Goourey, P. de Sainte Claire, L. Balan, Y. Israëli, Acrylate photopolymer doped with ZnO nanoparticles: an interesting candidate for photo-patterning applications, J. Mater. Chem. C 1 (2013) 3430-3438.

[24] A. Barichard, B. Mailhot, A. Rivaton, Y. Israëli, T. Galstian, Direct evidence of photo-induced diffusion of quantum dots in a photopolymerizable matrix, Nanotechnology 20 (2009) 255303-1-255303-4.

[25] G.G. Goourey, P. Wong-Wah-Chung, F. Jestin-Delor, B. Legeret, L. Balan, Y. Israëli, Photostability of acrylate photopolymers used as components in recording materials, Polym. Degrad. Stab. 119 (2015) 208-216.

[26] S. Chakrabarti, B. Chaudhuri, S. Bhattacharjee, P. Das, B.K. Dutta, Degradation mechanism and kinetic model for photocatalytic oxidation of PVC–ZnO composite film in a presence of a sensitizing dye and UV radiation, J. Hazard. Mater. 154 (2008) 230-236.

[27] D. Sil, S. Chakrabarti, Photocatalytic degradation of PVC-ZnO composite film under tropical sunlight and artificial UV radiation: A comparative study, Solar Energy 84 (2010) 476-485.

[28] C. Wilhelm, J.-L. Gardette, Infrared analysis of the photochemical behaviour of segmented polyurethanes: 1. Aliphatic poly(ester-urethane), Polymer 38 (1997) 4019-4031.

[29] X. Gu, G. Chen, M. Zhao, S.S. Watson, P.E. Stutzman, T. Nguyen, J.W. Chin, J.W. Martin, Role of nanoparticules in life cycle of ZnO/polyurethane nanocomposites, NSTI-Nanotech. 1 (2010) 709-712.

[30] X. Gu, D. Zhe, S.S. Watson, G.N. Chen, M. Zhao, D. Stanley, P.E. Stutzman, T. Nguyen, J.W. Chin, J.W. Martin, Studying Long-term Performance of a Nano-ZnO filled

Waterborne Polyurethane Coating using Spectroscopies and Microscopies, in: Coatings Science International, Noordwijk, The Netherlands, 2009.

[31] X. Gu, D. Zhe, M. Zhao, G. Chen, S.S. Watson, P.E. Stutzman, T. Nguyen, J.W. Chin, J.W. Martin, More durable or more vulnerable? – Effect of nanoparticles on long-term performance of polymeric nanocomposites during UV exposure, Int. J. Sustainable Materials and Structural Systems 1 (2012) 68-94.

[32] Z.Y. Wang, F.C. Liu, E.H. Han, W. Ke, S.Z. Luo, Effect of ZnO nanoparticles on anti-aging properties of polyurethane coating, Chin. Sci. Bull. 54 (2009) 3464-3472.

[33] G. Peng, Q. Li, Y. Yang, H. Wang, Degradation of nano ZnO-glass fiber-unsaturated polyester composites, J. Appl. Polym. Sci. 114 (2009) 2128-2133.

[34] S. Therias, J.-F. Larché, P.-O. Bussière, J.-L. Gardette, M. Murariu, P. Dubois, Photochemical behavior of polylactide/ZnO nanocomposite films, Biomacromolecules 13 (2012) 3283-3291.

[35] H. Zhao, R.K.Y. Li, A study on the photo-degradation of zinc oxide (ZnO) filled polypropylene nanocomposites, Polymer 47 (2006) 3207-3217.

[36] A. Ammala, A.J. Hill, P. Meakin, S.J. Pas, T.W. Turney, Degradation studies of polyolefins incorporating transparent nanoparticulate zinc oxide UV stabilizers, J. Nanopart. Res. 4 (2002) 167-174.

[37] R. Yang, Y. Li, J. Yu, Photo-stabilization of linear low density polyethylene by inorganic nano-particles, Polym. Degrad. Stab. 88 (2005) 168-174.

[38] R. Yang, P.A. Christensen, T.A. Egerton, J.R. White, Degradation products formed during UV exposure of polyethylene–ZnO nano-composites, Polym. Degrad. Stab. 95 (2010) 1533-1541.

[39] S. Musić, S. Popović, M. Maljković, D. Dragčević, Influence of synthesis procedure on the formation and properties of zinc oxide, J. Alloys Compd. 347 (2002) 324-332.

[40] D.A. Schwartz, N.S. Norberg, Q.P. Nguyen, J.M. Parker, D.R. Gamelin, Magnetic quantum dots: synthesis, spectroscopy, and magnetism of Co^{2+}- and Ni^{2+}-doped ZnO nanocrystals, J. Am. Chem. Soc. 125 (2003) 13205-13218.

[41] R.-O. Moussodia, L. Balan, C. Merlin, C. Mustin, R. Schneider, Biocompatible and stable ZnO quantum dots generated by functionalization with siloxane-core PAMAM dendrons, J. Mater. Chem. 20 (2010) 1147-1155.

[42] C. Madeleine-Perdrillat, F. Delor-Jestin, P.-O. Bussière, P. de Sainte-Claire, J.-F. Pilichowski, M. Baba, Simultaneous UV or thermal exposure and IR detection of evolved vapours: new tool for studying polymer photo-degradation, J. Photoch. Photobiol. A 278 (2014) 53-59.

[43] J.-F. Larché, P.-O. Bussière, P. Wong-Wah-Chung, J.-L. Gardette, Chemical structure evolution of acrylic-melamine thermoset upon photo-ageing, Eur. Polym. J. 48 (2012) 172–182.

[44] T. Kumazawa, X.-P. Lee, K. Sato, O. Suzuki, Solid-phase microextraction and liquid chromatography/mass spectrometry in drug analysis, Anal. Chim. Acta 492 (2003) 49–67.

[45] W.C. Oliver, G.M. Pharr, An improved technique for determining hardness and elastic modulus using load and displacement sensing indentation experiments, J. Mater. Res. 7 (1992) 1564-1583.

[46] A.-Y. Jee, M. Lee, Comparative analysis on the nanoindentation of polymers using atomic force microscopy, Polym. Test. 29 (2010) 95-99.

[47] I.N. Sneddon, The relation between load and penetration in the axisymmetric boussinesq problem for a punch of arbitrary profile, Int. J. Eng. Sci. 3 (1965) 47-57.

[48] D.J. Carlsson, R. Brousseau, C. Zhang, D.M. Wiles, Chapter 27-Identification of Products from Polyolefin Oxidation by Derivatization Reactions, in: J.L. Beham, J.F.

Kinstle (Eds.), Chemical Reactions on Polymers, ACS Symposium Series 364, American Chemical Society, Washington DC, 1988, pp. 376–389.

[49] S. Carroccio, P. Rizzarelli, C. Puglisi, MALDI Investigation of photooxidation in aliphatic polyesters: poly(butylene succinate), Macromolecules 37 (2004) 6576-6586.

[50] J. Bei, W. He, X. Hu, S. Wang, Photodegradation behavior and mechanism of block copoly(caprolactone-ethylene glycol), Polym. Degrad. Stab. 67 (2000) 375-380.

[51] C.Wilhelm, Mécanismes de photooxydation d'élastomères de polyurethannes thermoplastiques, Ph.D. Thesis, Université Blaise Pascal de Clermont-Ferrand, France, 1994.

[52] J.-L. Gardette, B. Mailhot, F. Posada, A. Rivaton, C. Wilhelm, Photooxidative degradation of polyether-based polymers, Macromol. Symp. 143 (1999) 95-109.

[53] J.F. Larché, P.-O. Bussière, S. Therias, J.-L. Gardette, Photooxidation of polymers: Relating material properties to chemical changes, Polym. Degrad. Stab. 97 (2012) 25-34.

[54] W.Y. Suprun, D. Kieβling, T. Machold, H. Papp, Oxidation of acetaldehyde and propionaldehyde on a VO_x/TiO_2 catalyst in the presence of water vapor, Chem. Eng. Technol. 29 (2006) 1376-1380.

[55] J.F. Larché, P.-O. Bussière, P. Wong-Wah-Chung, J.-L. Gardette, Chemical structure evolution of acrylic-melamine thermoset upon photo-ageing, Eur. Polym. J. 48 (2012) 172-182.

[56] G. Ragosta, M. Abbate, P. Musto, G. Scarinzi, Spectroscopic, mechanical and dynamic-mechanical studies on the photo-aging of a tetrafunctional epoxy resin, Macromol. Symp. 286 (2009) 34-41.

[57] A. Khajeh, F. Mustapha, M.T.H. Sultan, G. Bánhegyi, Z. Karácsony, V. Baranyai, The effect of thermooxidative aging on the durability of glass fiber-reinforced epoxy,

Advances in Materials Science and Engineering 2015 (2015) 1-13. http://dx.doi.org/10.1155/2015/372354

[58] H. Makki, N.S. Koen, K.N.S. Adema, E.A.J.F. Peters, J. Laven, L.G.J. van der Ven, R.A.T.M. van Benthem, G. de With, Degradation of a Polyester-Urethane Coating: Physical Properties, J. Polym. Sci.: Part B: Polym. Phys. 54 (2016) 659–671.

[59] A.Y. Jee, M. Lee, Comparative analysis on the nanoindentation of polymers using atomic force microscopy, Polymer testing 29 (2010) 95-99.

[60] K.N.S. Adema, Photodegradation of polyester-urethane coatings, Ph.D. Thesis, Eindhoven University of Technology, the Netherlands, 2015.

[61] J.-F. Larché, P.-O. Bussière, S. Thérias, J.-L. Gardette, Photooxidation of polymers : relating material properties to chemical changes, Polym. Degrad. Stab. 97 (2012) 23-34.

[62] S. Cho, W. Choi, Solid-phase photocatalytic degradation of PVC–TiO_2 polymer composites, J. Photoch. Photobiol. A: Chemistry 143 (2001) 221-228.

[63] A.A. Khodja, T. Sehili, Utilisation de l'énergie solaire dans le traitement des eaux : dégradation photocatalytique de micropolluants organiques en solution aqueuse, Rev. Energ. Ren. 1 (1998) 1-8.

[64] I. Izumi, W.W. Dunn, K.O. Wilbourn, F.-R.F. Fan, A.J. Bard, Heterogeneous photocatalytic oxidation of hydrocarbons on platinized titanium dioxide powders, J. Phys. Chem. 84 (1980) 3207-3210.

[65] G. Marque, Absorption de l'eau par les polymères, Ph.D. Thesis, Université de Savoie, France, 2009.

[66] I. Merdas, A. Tcharkhtchi, F. Thominette, J. Verdu, K. Dean, W. Cook, Water absorption by uncrosslinked polymers, networks and IPNs having medium to high polarity, Polymer 43 (2002) 4619-4625.

[67] Z. Chen, Q. Gu, H. Zou, T. Zhao, H. Wang, Molecular dynamics simulation of water diffusion inside an amorphous polyacrylate latex film, J. Polym. Sci.: Part B: Polym. Phys. 45 (2007) 884-891

[68] J.A. Burunkova, I.Yu. Denisyuk, S.A. Semina, Self-Organization of ZnO Nanoparticles on UV-curable acrylate nanocomposites, Journal of Nanotechnology 2011 (2011) doi: 10.1155/2011/951036, 1-6.

[69] A.B. Djurišić, W.C.H. Choy, V.A.L. Roy, Y.H. Leung, C.Y. Kwong, K.W. Cheah, T.K.G.R. Rao, W.K. Chan, H.F. Lui, C. Surya, Photoluminescence and electron paramagnetic resonance of ZnO tetrapod structures, Adv. Funct. Mater. 14 (2004) 856-864.

[70] Y. Liu, T. Morishima, T. Kawazoe, M. Ohtsu, Size control of sol–gel-synthesized ZnO quantum dots using photo-induced desorption, Nanotechnology 22 (2011) 215605-1-215605-5.

[71] M.L. Kahn, T. Cardinal; B. Bousquet, M. Monge, V. Jubera, B. Chaudret, Optical properties of zinc oxide nanoparticles and nanorods synthesized using an organometallic method, ChemPhysChem 7 (2006) 2392-2397.

[72] X. Xu, C. Xu, Z. Shi, C. Yang, B. Yu, J. Hu, Identification of visible emission from ZnO quantum dots: Excitation-dependence and size-dependence, J. Appl. Phys. 111 (2012) 083521-1-083521-6.

[73] A. van Dijken, E.A. Meulenkamp, D. Vanmaekelbergh, A. Meijerink, The luminescence of nanocrystalline ZnO particles: the mechanism of the ultraviolet and visible emission, J. Lumin. 87-89 (2000) 454-456.

[74] V. Subramanian, E.E. Wolf, P.V. Kamat, Green emission to probe photoinduced charging events in ZnO−Au nanoparticles, Charge distribution and Fermi-level equilibration, J. Phys. Chem. B 107 (2003) 7479-7485.

[75] A. Wood, M. Giersig, P. Mulvaney, Fermi level equilibration in quantum dot−metal nanojunctions, J. Phys. Chem. B. 105 (2001) 8810-8815.

[76] X. Gu, G. Chen, M. Zhao, S.S. Watson, T. Nguyen, J.W. Chein, J.W. Martin, Critical role of particle/polymer interface in photostability of nano-filled polymeric coating, J. Coat. Technol. Res. 9 (2012) 251-267.

[77] S. Ngo, L. M. Betts, F. Dappozze, M. Ponczek, C. George, C. Guillard. Kinetics and mechanism of the photocatalytic degradation of acetic acid in absence or presence of O_2. J. Photochem. Photobiol. A : Chem. 339 (2017) 80-88.

[78] L. M. Betts, F. Dappozze, C. Guillard. Undestanding the photocatalytic degradation by P25 TiO_2 of acetic acid and propionic acid in the pursuit of alkane production. Appl. Catal. A, General 554 (2018) 35-43.

[79] C. M. Rosado-Reyes, J. S. Francisco. Atmospheric oxidation pathways of acetic acid. J. Phys. Chem. A 110 (2006) 4419-4433.

Figure captions

Fig. 1. Monomers (a) Pentaerythritol tetraacrylate (PETTA) and(b) 2-(2-ethoxyethoxy)ethyl acrylate (2EEEA).

Fig. 2. (a) Infrared spectra waterfall and (b) changes in the infrared spectra of a PETTA/2EEEA film upon in situ irradiation at $\lambda \geq 300$ nm and 40 °C.

Fig. 3. (a) HS-SPME/GC-MS chromatogram of a PETTA/2EEEA film as a function of irradiation time in SEPAP 12/24 ($\lambda \geq 300$ nm, 40 °C). (b) Kinetic evolution of the area of the peak of ethanoic acid (H) and 2-(2-ethoxyethoxy)ethanol (J) stemming from the irradiation of a PETTA/2EEEA film.

Fig. 4. Proposed degradation pathways of 2-(2-ethoxyethoxy)ethanol initiated by H abstraction at positions 1and 2. PH designates 2EEEA units that contain hydrogen labile in the α position to respect to oxygen atom.

Fig. 5. (a) Force-displacement curves of PETTA/2EEEA polymer at 0, 50 and 300 hours of irradiation in SEPAP 14/24 ($\lambda \geq 300$ nm, 40 °C). (b) Kinetic evolution of calculated nano-hardness for a given force of 20 µN upon irradiation of PETTA/2EEEA polymer. Inset: Correlation between the nano-hardness and the decay of the residual vinyl groups (band at 1635 cm^{-1}).

Fig. 6 (a) Evolution of ATR-IR spectra of ZnO QD dispersed acrylate photopolymer (1 wt% of QDs) and (b) Comparison of kinetic evolution of the decay of the ester groups (band at

1724 cm^{-1}) for the pure and doped photopolymer (1 wt% of QDs). Inset: Correlation between the two bands of the ester groups of PETTA/2EEA photopolymer.

Fig. 7. (a) Comparison of HS-SPME/GC-MS chromatograms of a pure PETTA/2EEEA film and composite material films containing 1 or 5 wt% of ZnO QDs, after 10 and 150 hours of irradiation in SEPAP 12/24 ($\lambda \geq 300$ nm, 60 °C). (b) Evolution of the area of the peak corresponding to 2-(2-ethoxyethoxy)ethanol (J) as a function of the amount of QDs, for a given irradiation time.

Fig. 8. Kinetic evolution of formation of (a) ethanol (B) and (b) 2-(2-ethoxyethoxy)ethanol (J) stemming from the first hours of *in situ* irradiation ($\lambda \geq 300$ nm, 60 °C) and detected by GC-MS in dynamic mode.

Fig. 9. Proposed mechanism of formation of 2-(2-ethoxyethoxy)ethanol in the presence of ZnO involving hydroxyl radicals.

Fig. 10. (a) Excitation spectra of an irradiated PETTA/2EEEA film containing 1 wt% of ZnO QDs after storage in the dark at room temperature during 3 days. (b) For each irradiation time in SEPAP 14/24 ($\lambda \geq 300$ nm and 40 °C), evolution of the fluorescence intensity at 570 nm ($\lambda_{exc.} = 350$ nm) of a composite film after irradiation and followed with a storage during 1, 2 and 3 days in the dark. Inset: Correlation between the maximum fluorescence intensity value and the decrease of the ester groups (band at 1724 cm^{-1}).

Fig. 11. (a) Comparison of HS-SPME/GC-MS chromatograms of a pure PETTA/2EEEA film and composite material films containing ZnO QDs (5 nm) or ZnO NPs (10-30 nm) (loading 1

wt%), irradiated 150 h in SEPAP 12/24 ($\lambda \geq 300$ nm, 60 °C). (b) Evolution of the area of the peaks corresponding to 2-ethoxyethanol (E) and ethanoic acid (H) as a function of the size of ZnO nanoparticles.

Table 1

Main changes in the infrared spectra of PETTA/2EEEA polymer film after irradiation in a SEPAP 14/24 accelerated ageing device ($\lambda \geq 300$ nm, 40 °C).

Band consumption	Band formation
Residual vinyl groups of acrylate units:	
CH=CH (3037 cm^{-1})	
C=C (1635 cm^{-1})	CH_2 of polymer (2935 and
CH_2-CH=CH (1408 cm^{-1})	1452 cm^{-1})
2EEEA units:	O-H (3320 cm^{-1})
CH_2 (2870 cm^{-1})	
C-O-C (1115 $cm^{—1}$)	
Ester groups	C=O (1782 cm^{-1})
C=O (1736 cm^{-1})	
C-O (1188 cm^{-1})	

Table 2

Volatile organic compounds released from irradiated PETTA/2EEEA film as identified by HS-SPME/GC-MS. The labels used are the same that those cited in Ref. 25.

Retention time (min)	Confidence index (%)	Products
2.4	64	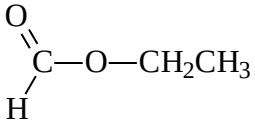 Ethyl formate (A)
4.0	91	CH_3CH_2OH Ethanol (B)
16.5	90	$HO\text{-}CH_2CH_2\text{-}O\text{-}CH_2CH_3$ 2-ethoxyethanol (E)
18.7	83	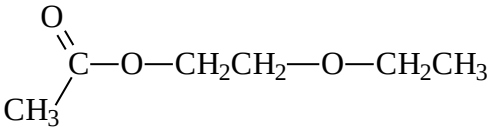 2-ethoxyethyl acetate (G)
21.8	91	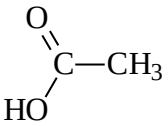 Ethanoic acid (H)
23.8	90	$HO\text{-}CH_2CH_2\text{-}O\text{-}CH_2CH_2\text{-}O\text{-}CH_2CH_3$ 2-(2-ethoxyethoxy)ethanol (J)

Table 3

For a constant load of 20 µN, comparison of the kinetic evolution of the nano-harness (expressed in MPa) of ZnO QD dispersed PETTA/2EEEA film with that of an undoped polymer film upon irradiation in a SEPAP 14/24 accelerated ageing device ($\lambda \geq 300$ nm and 40 °C).

Irradiation time (h)	QDs 0%	QDs 1%
0	40 ± 10	27 ± 1
3	191 ± 6	180 ± 10
20	270 ± 10	290 ± 10
50	330 ± 10	330 ± 10

Table 4

Influence of the size of ZnO nanoparticles on the initial rate of degradation.

ZnO nanoparticles	Initial rate (h^{-1})
0 %	5×10^{-3}
1 wt% of QDs (5 nm diameter)	9×10^{-3}
1 wt% of NPs (10-30 nm diameter)	0.5×10^{-3}

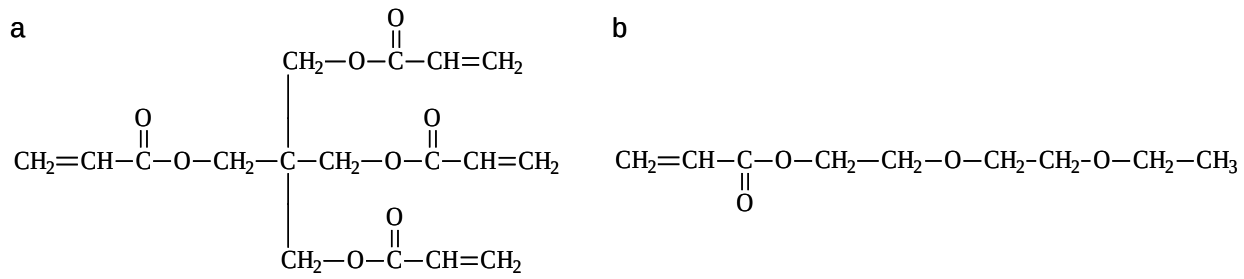

Fig. 1. Monomers (a) Pentaerythritol tetraacrylate (PETTA) and (b) 2-(2-ethoxyethoxy)ethyl acrylate (2EEEA).

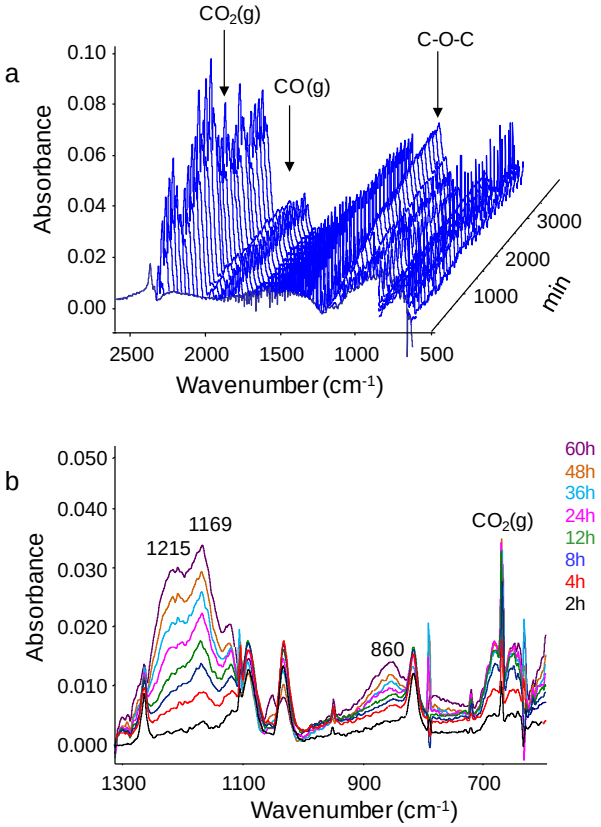

Fig. 2. (a) Infrared spectra waterfall and (b) changes in the infrared spectra of a PETTA/2EEEA film upon in situ irradiation at $\lambda \geq 300$ nm and 40 °C.

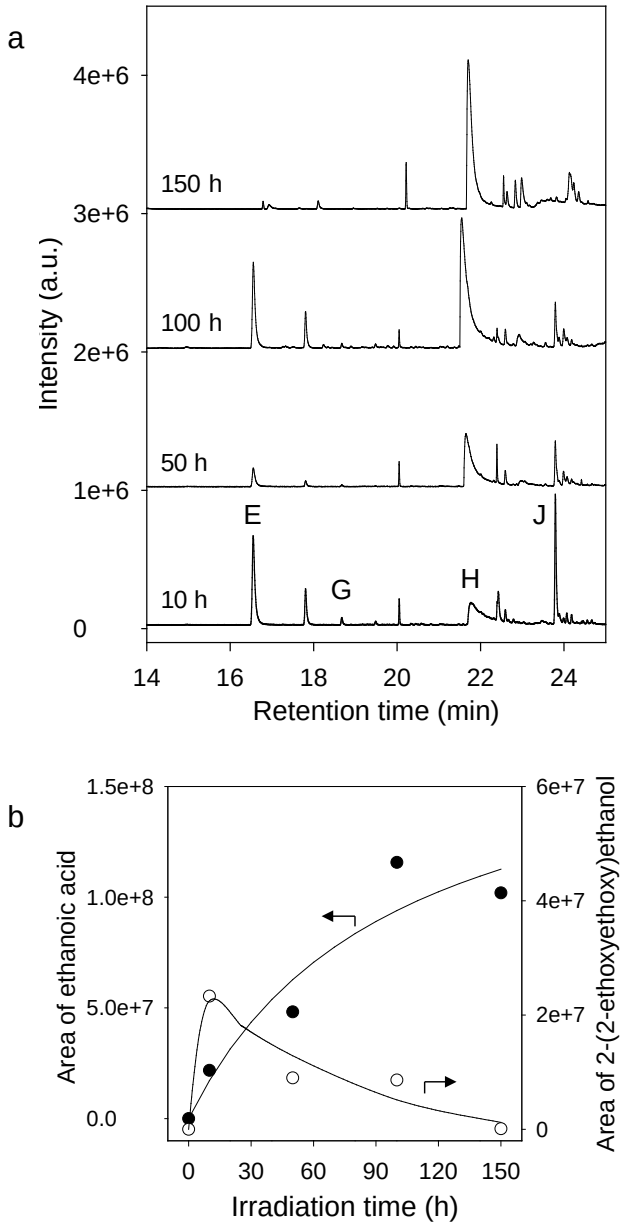

Fig. 3. (a) HS-SPME/GC-MS chromatogram of a PETTA/2EEEA film as a function of irradiation time in SEPAP 12/24 ($\lambda \geq 300$ nm, 40 °C). (b) Kinetic evolution of the area of the peak of ethanoic acid (H) and 2-(2-ethoxyethoxy)ethanol (J) stemming from the irradiation of a PETTA/2EEEA film.

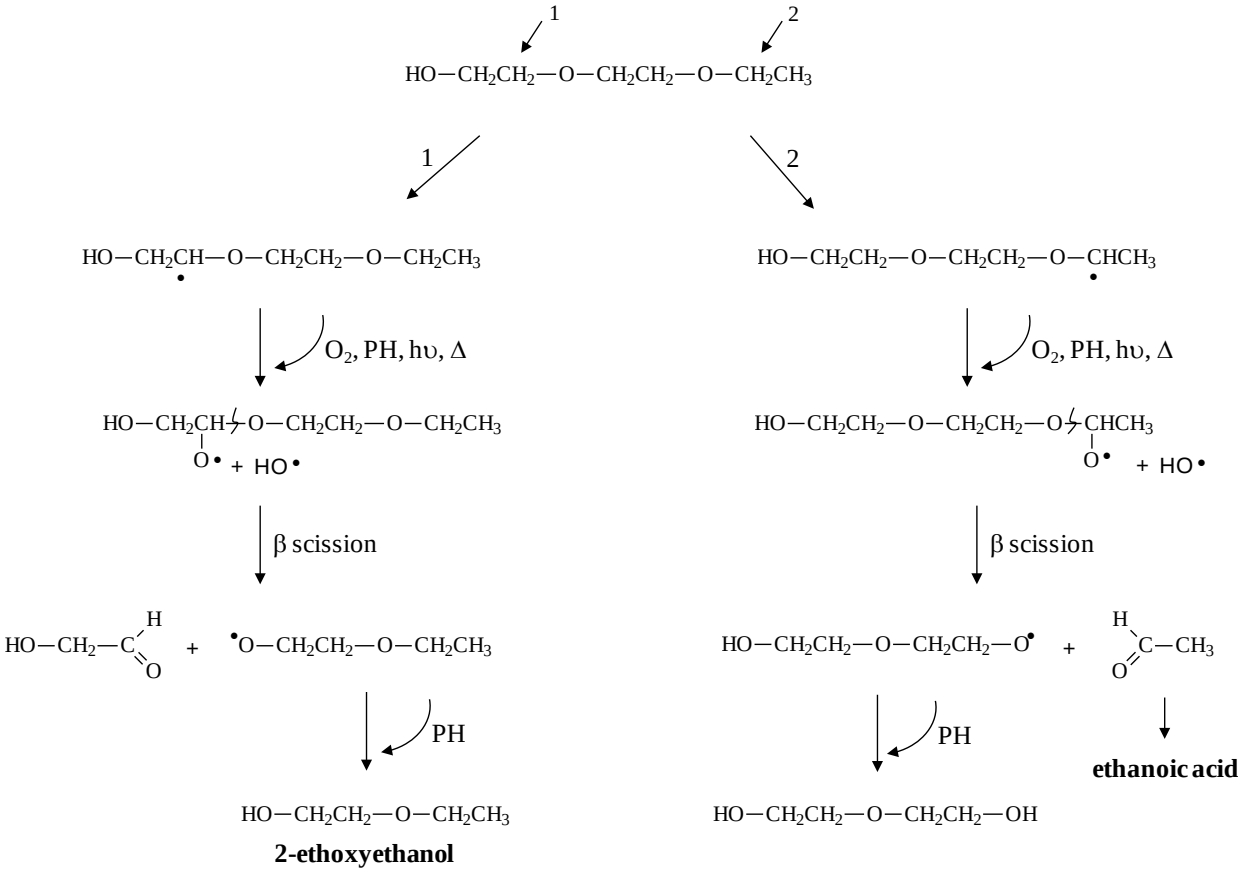

Fig. 4. Proposed degradation pathways of 2-(2-ethoxyethoxy)ethanol initiated by H abstraction at positions 1and 2. PH designates 2EEEA units that contain hydrogen labile in the α position to respect to oxygen atom.

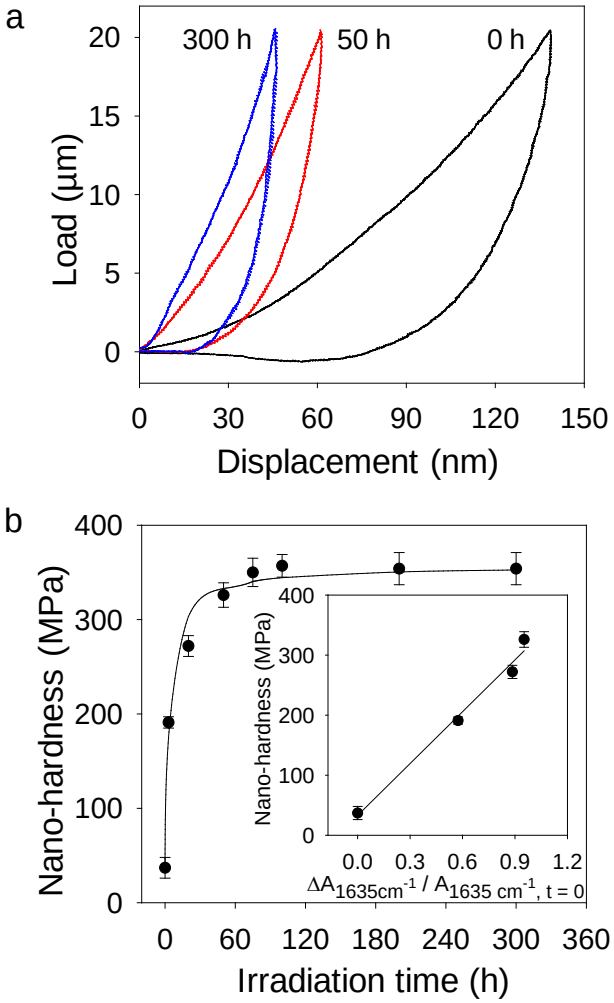

Fig. 5. (a) Force-displacement curves of PETTA/2EEEA polymer at 0, 50 and 300 hours of irradiation in SEPAP 14/24 ($\lambda \geq 300$ nm, 40 °C). (b) Kinetic evolution of calculated nano-hardness for a constant load of 20 µN upon irradiation of PETTA/2EEEA polymer. Inset: Correlation between the nano-hardness and the decay of the residual vinyl groups (band at 1635 cm^{-1}).

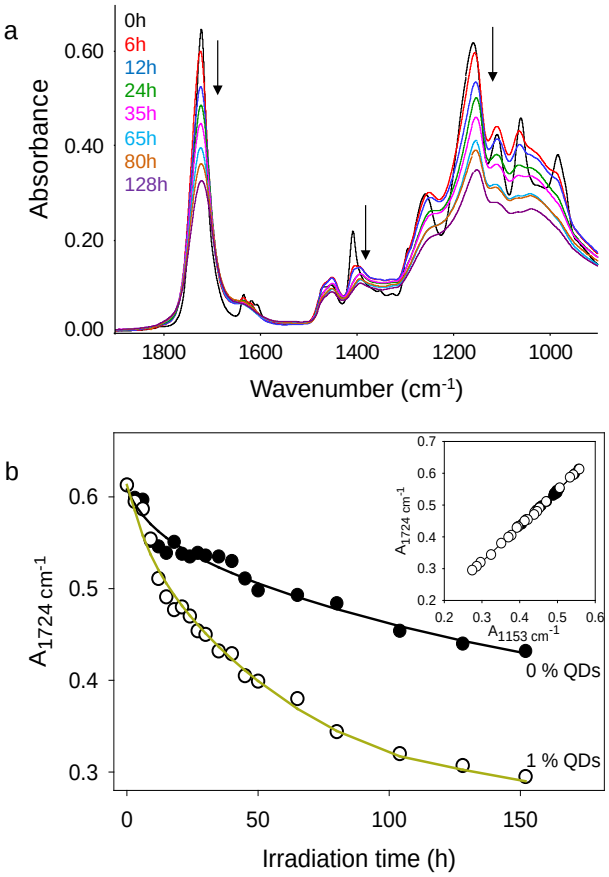

Fig. 6. (a) Evolution of ATR-IR spectra of ZnO QD dispersed acrylate photopolymer (1 wt% of QDs) and (b) Comparison of kinetic evolution of the decay of the ester groups (band at 1724 cm^{-1}) for the pure and doped photopolymer (1 wt% of QDs). Inset: Correlation between the two bands of the ester groups of PETTA/2EEA photopolymer.

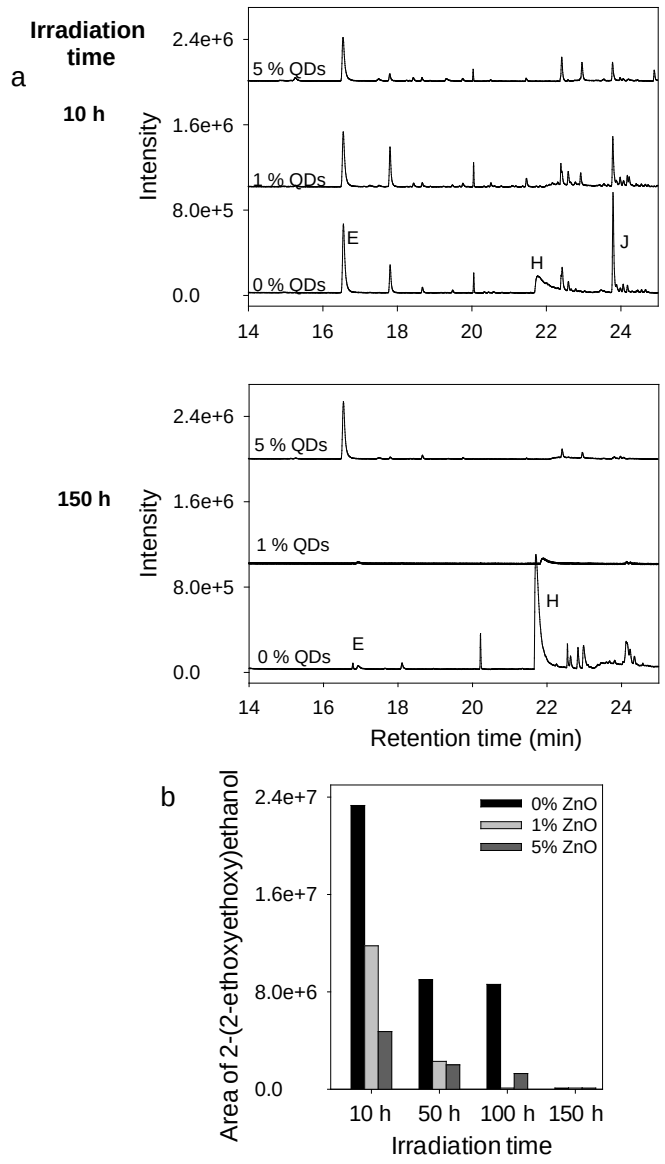

Fig. 7. (a) Comparison of HS-SPME/GC-MS chromatograms of a pure PETTA/2EEEA film and composite material films containing 1 or 5 wt% of ZnO QDs, after 10 and 150 hours of irradiation in SEPAP 12/24 ($\lambda \geq 300$ nm, 60 °C). (b) Evolution of the area of the peak corresponding to 2-(2-ethoxyethoxy)ethanol (J) as a function of the amount of QDs, for a given irradiation time.

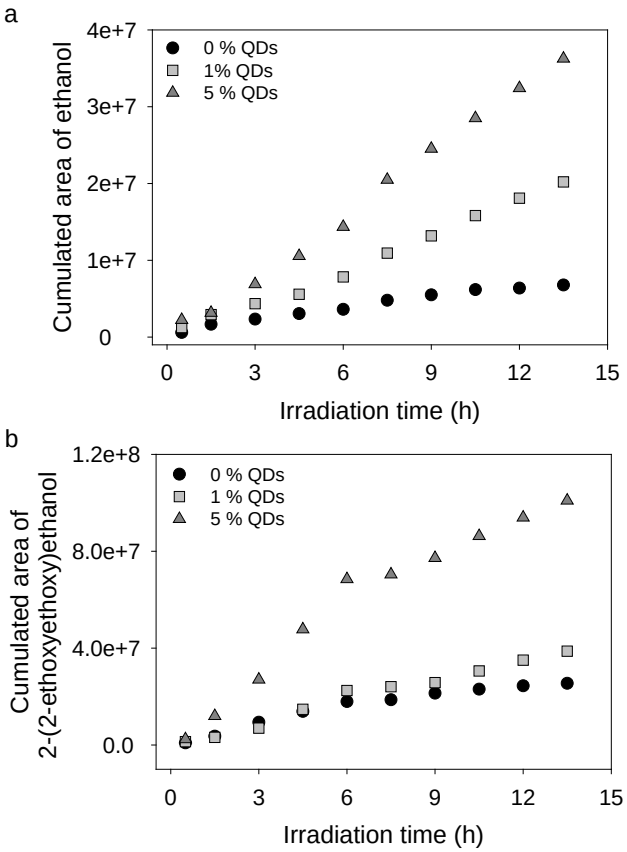

Fig. 8. Kinetic evolution of formation of (a) ethanol (B) and (b) 2-(2-ethoxyethoxy)ethanol (J) stemming from the first hours of *in situ* irradiation ($\lambda \geq 300$ nm, 60 °C) and detected by GC-MS in dynamic mode.

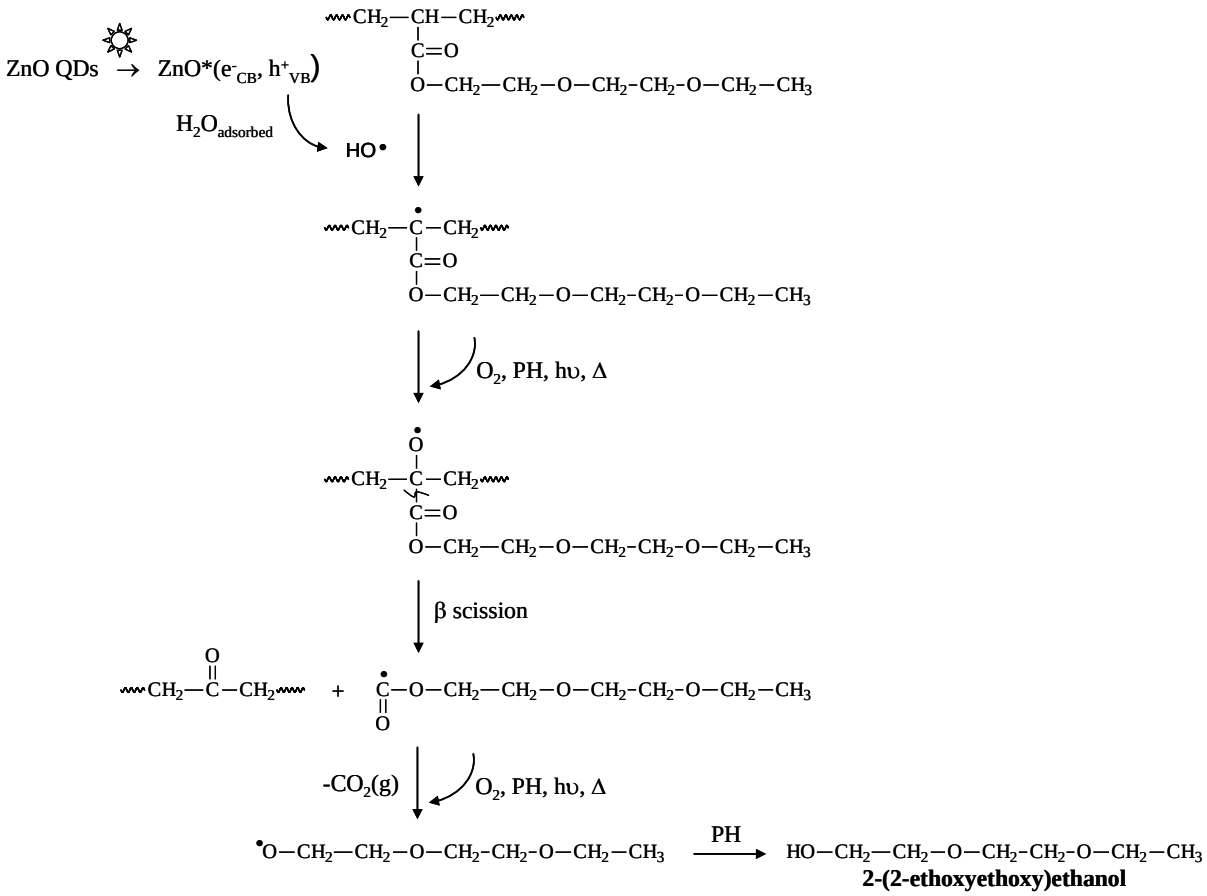

Fig. 9. Proposed mechanism of formation of 2-(2-ethoxyethoxy)ethanol in the presence of ZnO involving hydroxyl radicals.

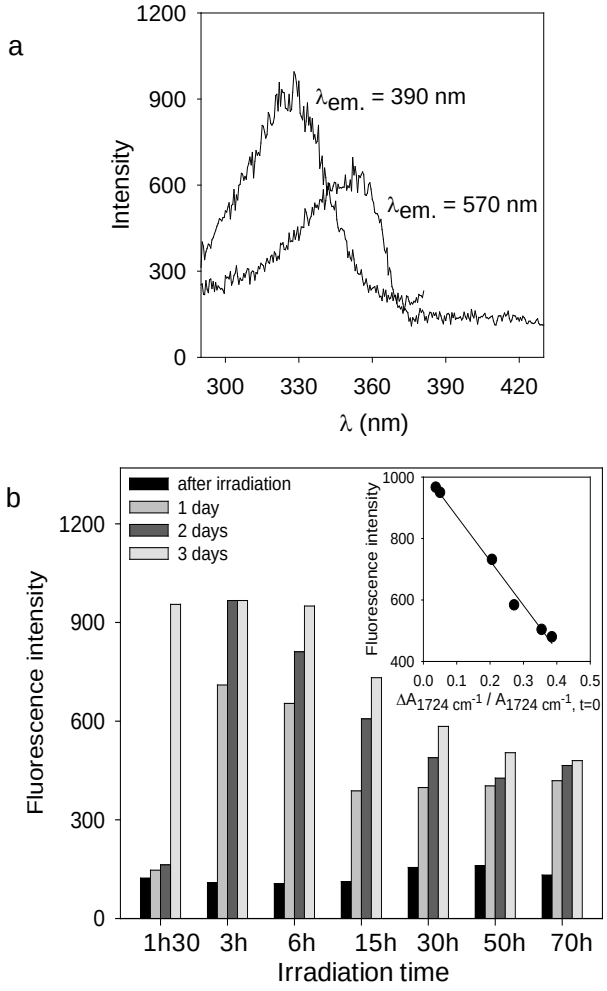

Fig. 10. (a) Excitation spectra of an irradiated PETTA/2EEEA film containing 1 wt% of ZnO QDs after storage in the dark at room temperature during 3 days. (b) For each irradiation time in SEPAP 14/24 ($\lambda \geq 300$ nm and 40 °C), evolution of the fluorescence intensity at 570 nm ($\lambda_{exc.} = 350$ nm) of a composite film after irradiation and followed with a storage during 1, 2 and 3 days in the dark. Inset: Correlation between the maximum fluorescence intensity value and the decrease of the ester groups (band at 1724 cm^{-1}).

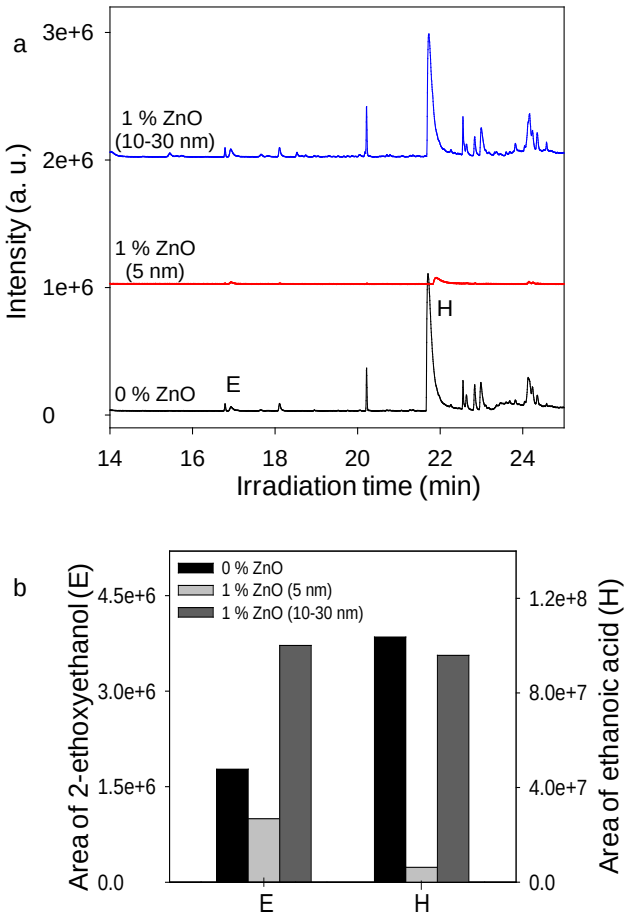

Fig. 11. (a) Comparison of HS-SPME/GC-MS chromatograms of a pure PETTA/2EEEA film and composite material films containing ZnO QDs (5 nm) or ZnO NPs (10-30 nm) (loading 1 wt%), irradiated 150 h in SEPAP 12/24 ($\lambda \geq 300$ nm, 60 °C). (b) Evolution of the area of the peaks corresponding to 2-ethoxyethanol (E) and ethanoic acid (H) as a function of the size of ZnO nanoparticles.

Graphical abstract

Effects of ZnO quantum dots on the photostability of acrylate photopolymers used as recording materials

Georgia G. Goourey, Pascal Wong-Wah-Chung, Lavinia Balan, Yaël Israëli

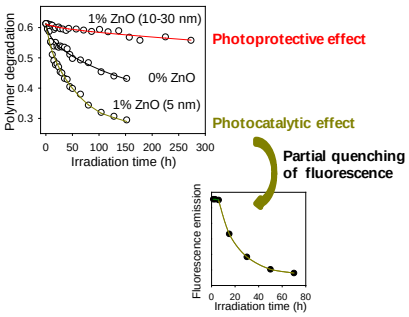

The photostability of ZnO/acrylate copolymer material under irradiation conditions simulating solar light strongly depends on the size of ZnO nanoparticles. Nanofillers with smaller size act as a photocatalyst involving the photogenerated charge carriers. This leads consequently to a partial quenching of their fluorescence. On the contrary, nanoparticles with bigger size play a photoprotective role towards the host polymeric matrix.